2020

Development Of A Computationally Inexpensive Method Of Simulating Primary Droplet Breakup

Brendon A. Cavainolo
University of Central Florida

DEVELOPMENT OF A COMPUTATIONALLY INEXPENSIVE METHOD OF SIMULATING PRIMARY DROPLET BREAKUP

by

BRENDON CAVAINOLO

A thesis submitted in partial fulfillment of the requirements
for the Honors in the Major Program in Aerospace Engineering
in the College of Engineering and Computer Science
and in the Burnett Honors College
at the University of Central Florida
Orlando, Florida

Fall 2020

Thesis Chair: Dr. Michael Kinzel

ABSTRACT

Liquid droplet impingement on aircraft can be problematic as it leads to ice accretion. There have been many incidents of aircraft disasters involving ice accretion, such as American Eagle Flight 4184. Understanding liquid droplet impingement is critical in designing aircraft that can mitigate the damages caused by icing. However, the FAA's regulations are only specified for "Appendix C" droplets; thus, aircraft designs may not be safe when accounting for droplets such as Supercooled Large Droplets. The assumptions of many models, such as the Taylor-Analogy Breakup (TAB) model, are no longer accurate for Supercooled Large Droplets, and the physics of those models break down. Computational modeling is used to simulate droplets in the SLD regime. A Lagrangian reference frame is used in this formulation. In this reference frame, a Volume of Fluid variation of the Navier-Stokes equations is used to resolve and isolate a single droplet. Experimental data shows conflicting results for Weber Number ranges in different primary breakup mechanisms. The goal of this research is to develop a computational model of a water droplet and test it against experimental data. This work shows that the scientific consensus on Weber Number ranges for different breakup modes may not necessarily be accurate, as the computational model agrees with some sets of experimental data but contradicts others.

This work is dedicated to all the people who have lost their lives in the COVID-19 pandemic and their grieving families, and to all the people suffering from the ensuing economic downturn.

ACKOWLEDGEMENT

I would like to thank Dr. Michael Kinzel for his mentorship during my time in his lab. He opened my eyes to the wonders and challenges of a career in research and encouraged me to continue this path. I also thank Dr. Andrew Dickerson for volunteering his time and guidance by on my thesis committee. I also thank Jason Turner and Dr. Douglas-Hector Fontes for their assistance in the initial stage of my research. I would not be here without their specific help and guidance. I thank all graduate and undergraduate researchers in the Computational Fluids and Aerodynamics Laboratory for their advice, criticism, and their inspirational work. I also thank the Excel/Compass program for starting me on my path to research as well as the Office of Honors Research and Office of Undergraduate Research for the funding they provided to me during this project.

TABLE OF CONTENTS

LIST OF FIGURES

LIST OF TABLES

LIST OF ABBREVIATIONS, ACRONYMS, AND NOMENCLATURE

AMR – Adaptive Mesh Refinement

CFD – Computational Fluid Dynamics

MVD – Mean Volumetric Diameter

SLD – Supercooled Large Droplet(s)

Oh – Ohnesorge Number

We – Weber Number

ρ – Density (kg/m^3)

σ – Surface Tension (N/m)

CHAPTER ONE: INTRODUCTION

Liquid droplet impingement on aircraft can be problematic for many reasons. Droplet impingement leads to icing on wings and in engines. Icing in engines can lead to structural damage, which compromises the safety of operating the vehicle. The icing on aircraft wings can compromise the aerodynamic properties of that wing, leading to inefficiencies and further complications with safety. Understanding liquid droplet impingement is critical in designing aircraft that can mitigate the damages caused by icing. One such case of catastrophic failure caused by ice accretion was seen in American Eagle Flight 4184 [1]. A flight with 68 people on board crashed into a field in Indiana. The National Transportation Safety Board issued an accident report, in which they stated the "probably cause" of the accident was a sudden hinge moment reversal after the deicing system failed to prevent ice accretion [1]. Another problem cited in the accident report was that the Federal Aviation Administration (FAA) failed to provide sufficient information on icing conditions, and thus, the FAA regulations were not sufficient to ensure flight safety [1]. These regulations are in context to droplets that have a mean volumetric diameter (MVD) of 50 μm or less, which are typically referred to as "Appendix C droplets" [2].

In practice, however, this classification of droplet is far from the only contributor to aircraft ice accretion. According to a study done by the FAA and NASA Glenn Research Center, Supercooled Large Droplets (SLD) exist in much higher quantities than previous data suggested [3]. Supercooled Large Droplets are a classification of droplets with MVD ranges from 50 μm to 3000 μm. These droplets are similar to rain droplets in terms of size. Internal temperatures of SLD can reach temperatures of -37.5˚C, while still maintaining a liquid state [4].

The assumptions of many models are no longer accurate for droplets in the SLD regime, as the physics of those models break down [4]. However, some broad numerical methods exist for predicting ice accretion on wings. One notable computational tool for this is the LEWis ICE accretion program (LEWICE). LEWICE predicts aircraft icing by coupling fluid dynamics and freezing models [5]. However, most of these tools share the same general methods. These methods include a CFD flow field calculation using multiphase physics, particle trajectory analysis and impingement calculation using the multiphase physics and set wall criteria, using flight conditions to determine the thermodynamic state of the droplets and ice growth as well as modifying the geometry in question to account for the ice growth [5].

Another important tool for use in predicting ice accretion is the Dispersed-Multiphase Model coupled with the Freezing-Boiling Model in Star-ccm+ [6]. Star-ccm+ is a powerful computational tool in this case because data from the Dispersed-Multiphase Model can be used for simulations in other reference frames. One such reference frame is the use of a Volume-of-Fluid (VOF) model to achieve a high-fidelity model of a droplet as it approaches a body [6]. The Dispersed-Multiphase Model is comprised of two phases. Air is the primary phase, while water is the secondary phase.

Recently, the spread of COVID-19 has the scientific community working on understanding person-to-person disease transmission in order to devise proper social distancing and mask guidelines. Droplet breakup plays a role in the spread of disease through respiratory droplets. Understanding the breakup modes of droplets of varying MVD can shed light on droplet distribution in cough and sneeze sprays. Droplets from healthy people are more akin to “Appendix C” droplets. The distribution of droplet size in a typical cough is shown to be multimodal, with

peaks at 1μm, 2μm, and 8μm [7]. However, work done by Scharfman [8] shows that coughs and sneezes can eject mucosalivary ligaments ranging in diameter from 0.409 mm to 0.952 mm, making them of similar size to droplets in the SLD regime, though their physical properties are much different. These drops are mostly water but contain mucous and other respiratory particles. While this project does not fully explore respiratory droplets, exploring transient properties of SLDs forms a basis for modeling more complicated fluids.

A parameter known as the Weber Number (*We*) is used in conjunction with analysis of 2D and 3D models to predict the breakup mode of the water droplet. The Weber Number is defined as the ratio of inertial forces tearing apart the droplet to the surface tension of the droplet, which is represented in Equation 1 below [9]. Another dimensionless parameter, the Ohnesorge Number (*Oh*), is used to determine whether the Weber Number is useful for predicting the breakup mode of the droplet in question. Ohnesorge Numbers that are less than 0.1 indicate that the viscous forces of the droplet are negligible [10]. The dimensionless relationship described by the Ohnesorge Number is shown below as Equation 2.

$$We = \frac{\rho_f v^2 D}{\sigma} \tag{1}$$

$$Oh = \frac{\mu}{\sqrt{\rho_l \sigma D}} \tag{2}$$

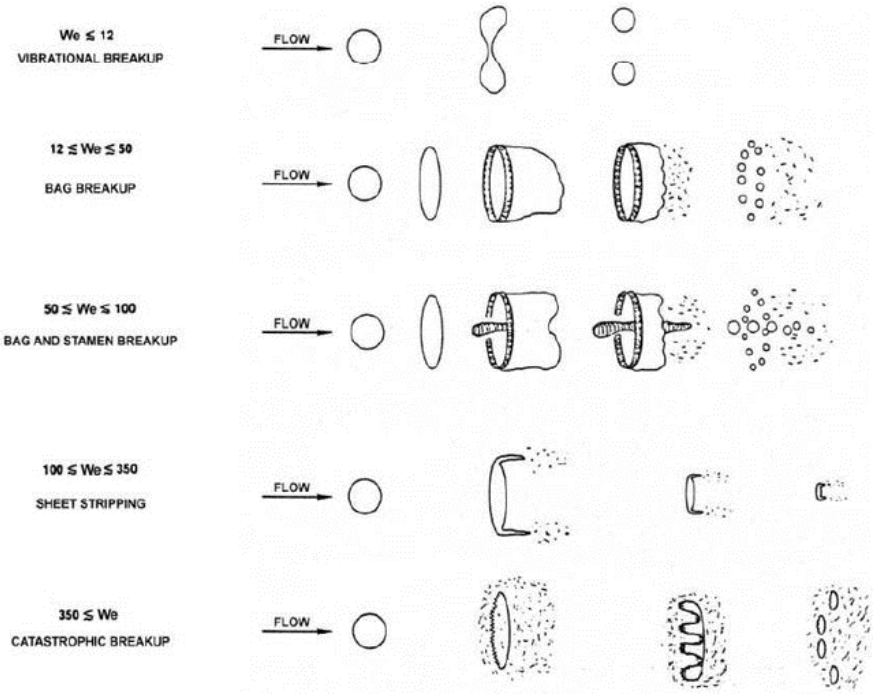

Figure 1: Droplet Breakup Modes with Approximate We Ranges [9]

A critical Weber Number is the Weber Number at which the droplet becomes unstable and begins to break up [9]. There are several types of droplet breakup, which are visualized in Figure 1 above.

Vibrational breakup occurs at lower Weber numbers as the droplet splits itself into several smaller droplets [11]. Droplets will eventually experience vibrational breakup at slower speeds. Bag breakup can be compared to a bubble popping while still attached to a bubble wand. Other types of breakup include sheet stripping, wave crest stripping, and catastrophic breakup. Each of these breakup modes occur within a specified range of Weber numbers. Violent flows imply a high Weber Number and thus lead to more violent droplet breakup [12]. Subsonic flights, being at lower speeds, are more likely to encounter droplets undergoing vibrational, bag, and bag-and-stem breakup. Supersonic flights are more likely to cause catastrophic breakup as the droplets encounter

a shock. It is still not clear what kind of breakup a hypersonic flight would encounter. The Weber Number ranges shown in Figure 1 are still under scrutiny. One such example is that vibrational breakup can occur at any Weber Number; it is not limited to the range shown above. Another example of discrepancies in previous work is in a paper on droplet breakup in a shock induced cross-flow where the range of Weber Numbers from 20 to 100 is considered “multi-mode” instead of bag/bag-and-stamen [13].

CHAPTER TWO: METHODOLOGY

Explanation of Methodology

The water droplets are simulated using Star-ccm+, a commercial Computational Fluid Dynamics Code developed by CD-Adapco and Siemens. Some simulation methods, such as the one used in a thesis published at Pennsylvania State University [12], use two coupled simulations to more accurately describe properties of droplets as they reach airfoils. In this case, both simulations employ the Eulerian Multiphase method of simulating more than one phase in a region. One key difference between these simulations is the reference frame. For the first simulation step, an Eulerian reference frame is used, meaning that the fluid is moving over a static symmetric airfoil, and the fluid is tracked as a continuous phase rather than an individual droplet. The streamline data from where the droplet hits the leading edge of the airfoil is extracted and converted to time-varying velocity data. This data is then imported into the second simulation. The second simulation, or the microscale simulation, is in the Lagrangian reference frame, meaning now an individual fluid particle is being tracked as it moves through the fluid domain. While this coupled method is effective in determining the breakup mode of the droplet, it requires running two simulations for each case and is more involved in terms of what Star-ccm+ needs to do.

This experiment focuses on the microscale simulation described in Turner's paper [12]. For this simulation to be carried out, specific models and parameters must be picked in Star-ccm+. For this method, all properties of the droplet are fixed except for the surface tension coefficient. Fixing the properties is useful because only one region needs to be created for all cases. The values

for the properties used here are a 100-micron diameter droplet, a density of 997.561 $\frac{kg}{m^3}$ and a 100 $\frac{m}{s}$ flow speed.

Geometry

Firstly, a region must be created for the particle to exist. This region can be a simple box shape part created using CAD or the built-in geometry functionality in Star-ccm+. The box should be around three times taller than the diameter of the droplet to keep the droplet breakup from flowing out of the region. The length of the box should be around ten times the droplet diameter to avoid reverse flow at the outlet, and the region should extend in the +x and +y directions. For the axisymmetric simulation, the length in the z-direction does not matter. However, it is important to have a symmetry plane at z=0 since this is the dimension Star-ccm+ uses to convert the geometry to 2D. For the 3D simulations, the region should extend from the origin in both -z and +z directions. The overall length should be three times the length of the droplet diameter to avoid pressure correction limitations.

Physics

At first, the 3D model is selected in the Physics Continuum, which will be converted to 2D, and eventually axisymmetric for the first part of this study. For the simulation phases, the Eulerian Multiphase Model is chosen since the simulation involves both air and water. Then, the implicit unsteady solver is selected to resolve the droplets in a time-varying frame. The Volume-

of-Fluid (VOF) model is selected, which is what allows the specification of the volume fraction of each Eulerian Phase. Multiphase Interaction is also automatically selected, so the model for this must be specified as well. A new Phase Interaction is created, and the VOF-VOF Phase Interaction model is specified. Multiphase Material and Surface Tension Force must also be selected for the surface tension to be set. This surface tension coefficient is essential for the Weber Number Calculation and is the independent variable for these studies. For simplicity in calculations, the laminar flow model is selected. This selection eliminates the need to evaluate which turbulence model would be better and eliminates the error associated with each turbulence model. The laminar selection is justified by water droplets having low Reynold's Numbers. The only optional model that is selected is the segregated fluid isothermal model in order to ensure that the two VOF phases are at the same temperature.

Meshing

In creating a computationally inexpensive way to simulate droplets, it is vital to keep in mind how many cells a mesh has and to make sure the machine the simulation is running on can handle the mesh fidelity. The preliminary 2D simulations shown below used a uniform mesh where the maximum cell size was $1/100^{th}$ of the droplet MVD. For the 3D simulations, a uniform mesh would not be optimal as computational power would be wasted on smaller cells toward the outlet. To fix this problem in 3D, the base size of the mesh should be set to $1/10^{th}$ the size of the droplet diameter and adaptive mesh refinement (AMR) should be enabled. AMR allows the mesh to shift according to a user-specified field function. In this case, the field function that AMR should

follow is the Volume fraction of water. AMR should be set to refine the mesh where the volume fraction of water is between 0.05 and 1.0. The transition width should be set to 10 cells to capture the changing velocities around the droplet accurately. AMR should also be set to three or four levels of refinement depending on the computational power of the machine being used to run the simulation. One drawback of AMR according to an analysis of automated moving mesh techniques done by Profir, is that this method introduces interpolation error [15]. The AMR model is seen below in

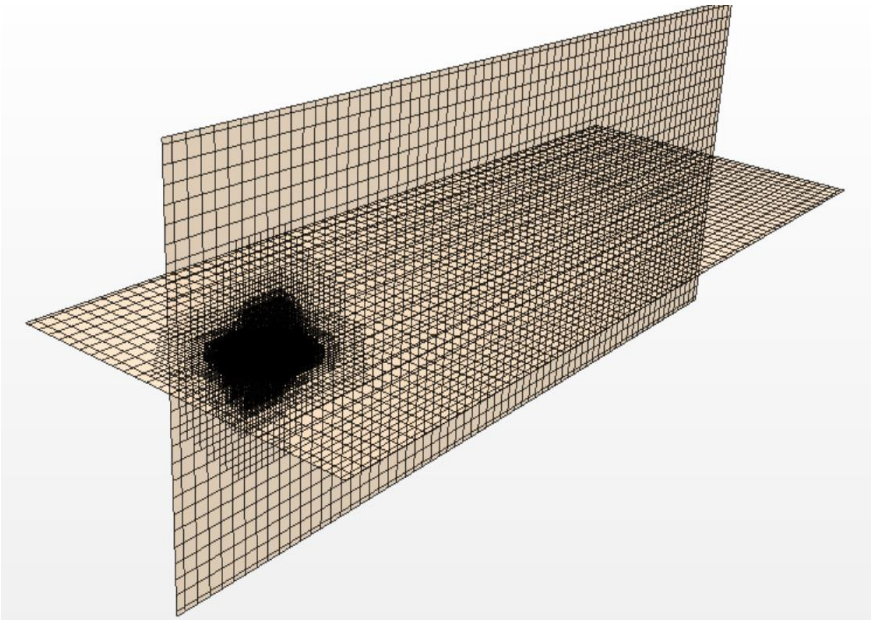

Figure 2: Adaptive Mesh Refinement Around Droplet

Initial Conditions

Firstly, a parameter is created that specifies the initial droplet radius (IDR). A field function (RAD) is created that specifies the center of the droplet. In order to maintain the axisymmetric model, the y-coordinate of the center must be zero. Another field function (INIT_LIQ) is created

that uses conditional formatting to set the volume fraction of water to 1.0 (fully water) if RAD is less than IDR, and to 0.0 (no water) if RAD is greater than IDR. One more field function must be created (INIT_AIR) to specify that the cells that are not water should be air. An example of these functions is shown below for a droplet of radius 50μm.

Table 1: Explanation of Field Functions

RAD	sqrt(pow($${Position}[0]-0.00005,2)+pow($${Position}[1],2)+pow($${Position}[2],2))
INIT_LIQ	${RAD}>${IDR}?0.0:1.0
INIT_AIR	1-${INIT_LIQ}
AIR_VEL	${VolFracWater}>0?100:0

Another vector field function (AIR_VEL) is created to specify the velocity of the air around the droplet. The if-else statement ensures the droplet is initially stationary while the air flows at 100 m/s. For the initial velocity condition, this AIR_VEL field function is selected. Also, in the initial physics conditions, a composite volume fraction must be specified. The first component of this composite volume fraction should be the air, it should specify a field function rather than a constant, and the INIT_AIR field function should be selected. The second component should be water, and the INIT_LIQ field function should be chosen. The initial pressure should be less than 1 atm to simulate stratospheric conditions.

Boundary Conditions

For the preliminary 2D simulations, the mesh must be converted from 3D to axisymmetric. Going from 3D to axisymmetric requires a mesh conversion to 2D using Star-CCM+'s built-in

conversion functionality. Deleting the old 3D region and physics continuum is an essential step in making sure the simulation runs appropriately. Once the mesh converts to 2D, the Two-dimensional model in the new Physics 2D continuum should be changed to the Axisymmetric model. From here, the boundaries need to be set to their appropriate type. One of the side boundaries needs to be a velocity inlet where 100 $\frac{m}{s}$ is specified as the velocity, and the volume fraction set to [1.0,0.0] (only air) for this boundary. The boundary on the other side must be a regular outlet. The top of the region should be a symmetry plane, and the bottom should be the axis. The axis is what makes the simulation axisymmetric because it revolves the region around that axis to form a pseudo-3D model.

For the 3D simulations, the 3D geometry is directly converted to a region. The inlet and outlet are in the same places as the axisymmetric simulation and have the same properties as well. All other boundaries are symmetry planes.

Data Collection and Viewing the Simulation

The only parameter that will be varied throughout the simulations is the surface tension coefficient σ. Since Weber Number is a dimensionless parameter, any of the variables in it can be changed to see the breakup modes for the Weber Number ranges. The surface tension coefficient is the easiest variable to change so that cases do not have to be run for changing velocities and changing droplet diameters. The surface tension coefficients used will be ones with corresponding Weber Numbers close to the suggested limits of each range seen in Figure 01 to see the sensitivity

in the change, as well as Weber Numbers well within each range to verify the accuracy of the model.

For a view of the water droplet as it moves through the region in the axisymmetric model, a new scaler scene should be created, and the "Volume Fraction of Water" field function should be set as the active displayer in that scene. Since the scene will only show the top half of the flow region, the region is mirrored about the x-axis to make it look like a cross section of a 3D flow. For the 3D simulations, the viewing method is a little less intuitive. The more computationally inexpensive approach involves creating two plane derived parts. One plane section should be coincident to the xy-plane, and the other should be coincident to the xz-plane. The more computationally expensive method is to use isosurfaces. These are surfaces generated for specified values of field functions. In this case, the volume fraction of water is the specified field function. The simulations used for these studies used three isosurfaces at volume fractions of 0.1, 0.5, and 0.95. There is a tradeoff here because using more isosurfaces makes a more accurate view of the droplet, but also causes increased computation time for rendering. The opacity on the isosurface should be set to 0.9 so that all the isosurfaces can be seen at once. From preliminary simulations, droplets experience primary breakup before 50μs, so this can be used as the stopping criterion for the droplet.

CHAPTER 3: RESULTS

Table 2: 2D Compressible Results Summary

Surface Tension, σ	Weber Number, *We*	Ohnesorge Number, *Oh*	Expected Breakup Mode	Resultant Breakup (Compressible)
0.002222222	573.93000	0.03986	Catastrophic	Sheet Stripping + Catastrophic
0.009777781	130.43860	0.01900	Sheet Stripping	Sheet Stripping
0.012444444	102.48750	0.01684	Sheet Stripping	Sheet Stripping
0.014222223	89.67656	0.01576	Bag/Stamen	Sheet Stripping
0.018666667	68.32500	0.01375	Bag/Stamen	Bag + Sheet Stripping
0.02311111	55.18558	0.01236	Bag/Stamen	Bag (Multi-mode)
0.027555554	46.28468	0.01132	Bag	Bag (Multi-mode)
0.036444477	34.99570	0.00984	Bag	Bag (Multi-mode)
0.071999995	17.71389	0.00700	Bag	Vibrational + Bag
0.100888889	12.64163	0.00592	Bag	Vibrational + Bag
0.120888933	10.55018	0.00540	Vibrational	Vibrational + Bag
0.222222222	5.73930	0.00399	Vibrational	Vibrational
0.444545138	2.869	0.00282	Vibrational	No Breakup

Table 2 shows the Weber Numbers for each simulation case. These Weber Numbers indicate the theoretical droplet breakup mode based on Figure 1, and they were calculated from Equation 1. In Equation 1, ρ_f is air in this case, and is constant at 1.2754, v is fixed at 100, D is the MVD of the droplet and is fixed at 100 μm, The surface tension coefficient is varied to change the droplets' Weber Number. Equation 2 was also used to calculate the Ohnesorge Number for each case to ensure that all the droplets' breakup modes can be accurately predicted by their Weber Number. Since all the cases present had Ohnesorge Numbers less than 0.1, the Weber Number is

an accurate predictor for all cases. Table 2 indicates that vibrational breakup occurs as a secondary breakup mode alongside other breakup modes and not just for cases where $We < 12$. This phenomenon is especially true for bag breakup on the lower end of the range suggested by Figure 1. A similar phenomenon is shown for sheet stripping at higher-end values for the bag-and-stamen breakup range indicated by Figure 1. Weber numbers closer to 100 are more likely to exhibit bag breakup as well as sheet stripping. Simulations in the bag-and-stamen breakup range seem not to present the stamen.

Table 3: 2D Incompressible Results Summary

Surface Tension, σ	Weber Number, We	Ohnesorge Number, Oh	Expected Breakup Mode	Resultant Breakup
0.002	573.93000	0.03986	Catastrophic	Sheet Stripping + Catastrophic
0.022	130.43860	0.01900	Sheet Stripping	Sheet Stripping
0.023	55.18558	0.00984	Bag and Stamen	Multi-mode (maybe stamen)
0.072	17.71389	0.00700	Bag	Vibrational + Bag
0.121	10.55018	0.00540	Vibrational	Vibrational + Bag
0.500	5.73930	0.00399	Vibrational	None

Table 3 shows some discrepancies between the compressible and incompressible results for 2D droplets. One of the biggest discrepancies here is the difference in bag breakup. Bag breakup does occur in compressible flow, but it does not occur in incompressible flow. The reason for this is not clear, but perhaps compressibility effects cause a shift in the ranges presented in Figure 1.

Table 4: 3D Incompressible Results Summary

Surface Tension, σ	Weber Number, We	Ohnesorge Number, Oh	Expected Breakup Mode	Resultant Breakup
0.002	573.93000	0.03986	Catastrophic	Sheet Stripping + Catastrophic
0.022	130.43860	0.01900	Sheet Stripping	Sheet Stripping
0.023	55.18558	0.00984	Bag and stamen	Multi-mode (maybe stamen)
0.072	17.71389	0.00700	Bag	Bag
0.500	5.73930	0.00399	Vibrational	None

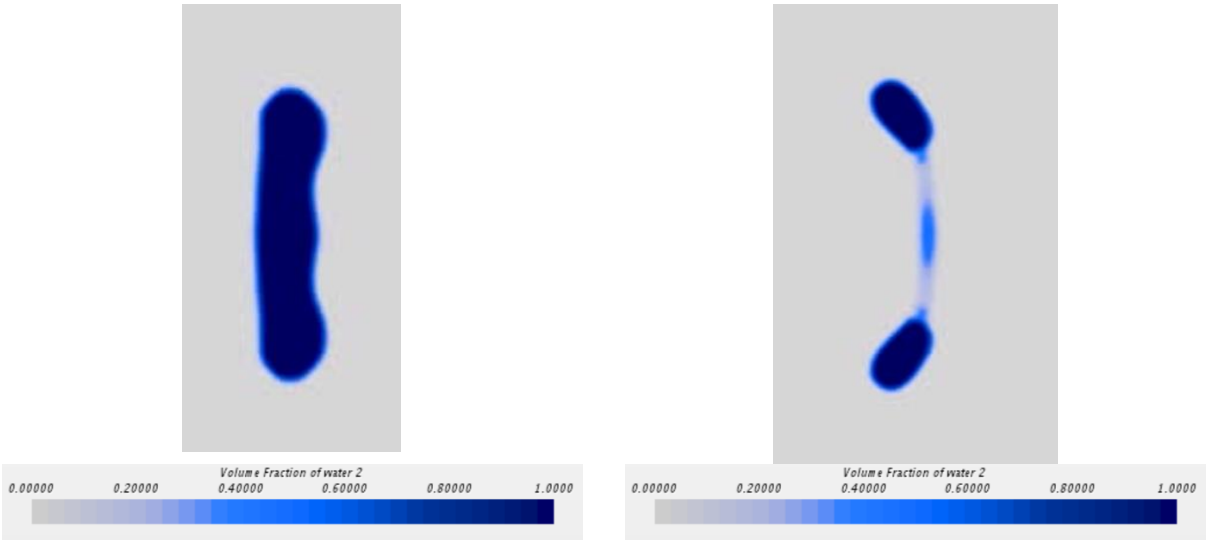

Figure 3: Example of Vibrational Breakup in Compressible Gas (We: 5.7393, Solution time: 15μs to 27.5μs)

The example shown in Figure 3 above is a droplet within the vibrational breakup regime of Weber Numbers from Figure 1. Qualitatively, this droplet shows properties of the vibrational breakup mode because a larger droplet deforms and breaks up into smaller droplets. One can imagine a full 2D simulation where the droplet in Figure 3 is reflected across the x-axis, showing two daughter droplets instead of the single daughter droplet shown in this axisymmetric case.

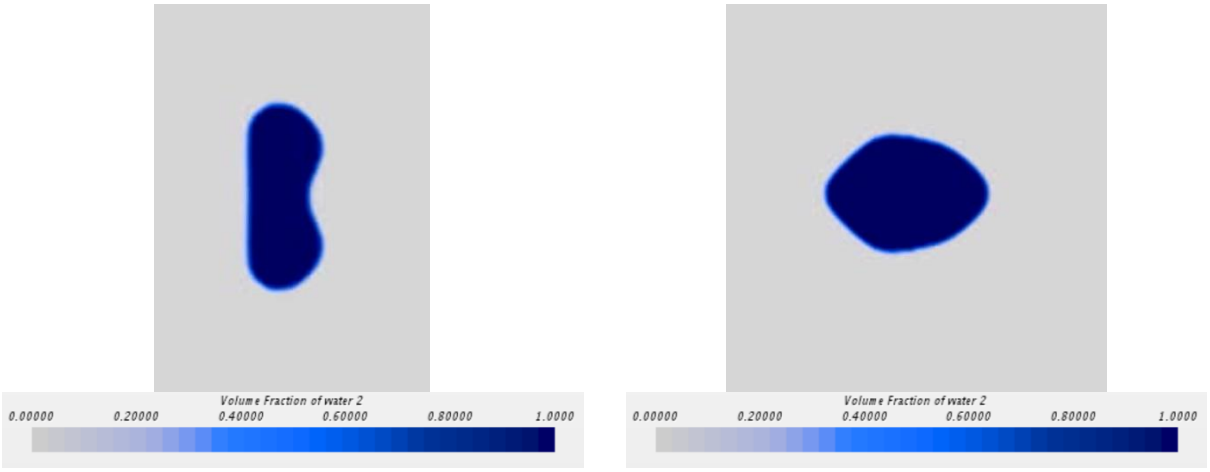

Figure 4: Example of Vibrational Breakup Regime in Incompressible Gas (We: 5.7393, Solution time: 18μs to 45μs)

Figure 4 shows a droplet with the same Weber Number as Figure 3, but in an incompressible gas domain. However, this droplet did not experience any form of breakup. Rather the droplet stretched out and bounced back like a rubber band.

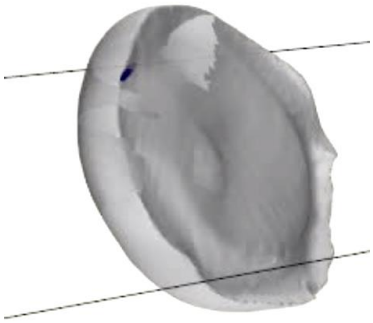

Figure 5: Example of Vibrational Breakup Regime in 3D Incompressible Gas (We: 5.7393, Solution time: 18μs)

Figure 5 shows a 3D model of the droplet presented in Figure 3 and Figure 4. The 3D model immediately shows a problem with using isosurfaces to view the droplet. When the volume fraction changes, parts of the droplet disappear in the scene even though they are still there.

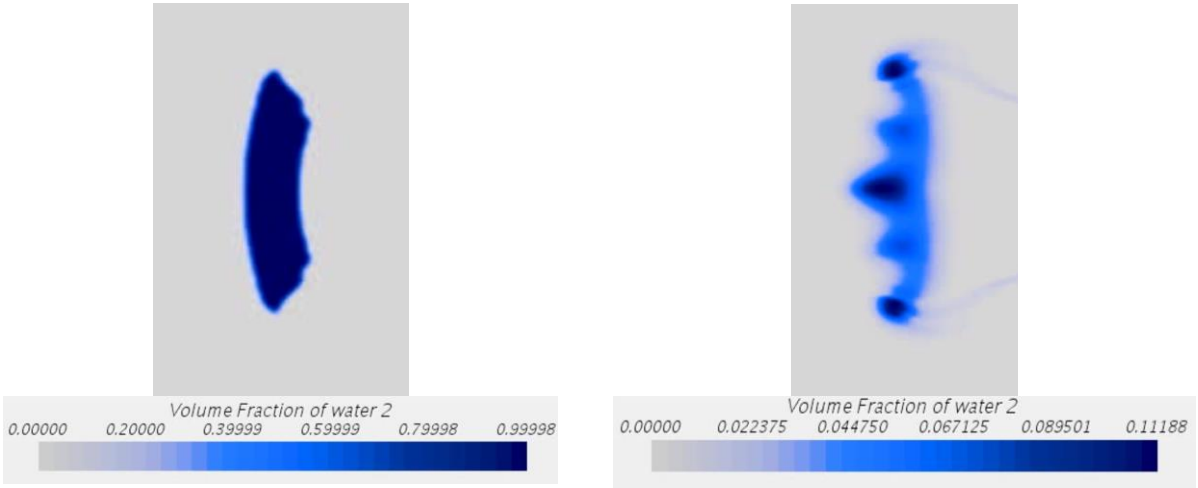

Figure 6: Example of Bag Breakup Regime in Compressible Gas (We: 17.7139, Solution time: 12μs to 34μs)

The example shown in Figure 6 above shows a droplet undergoing a mix of vibrational breakup and bag breakup. However, the focus is on the bag. The bag breakup mode is qualitatively seen in the dramatic decrease in the maximum volume fraction of water in the second image. A small stream of water coming from the top and bottom of the deformed droplet in the second image seem to show the formation of the bag.

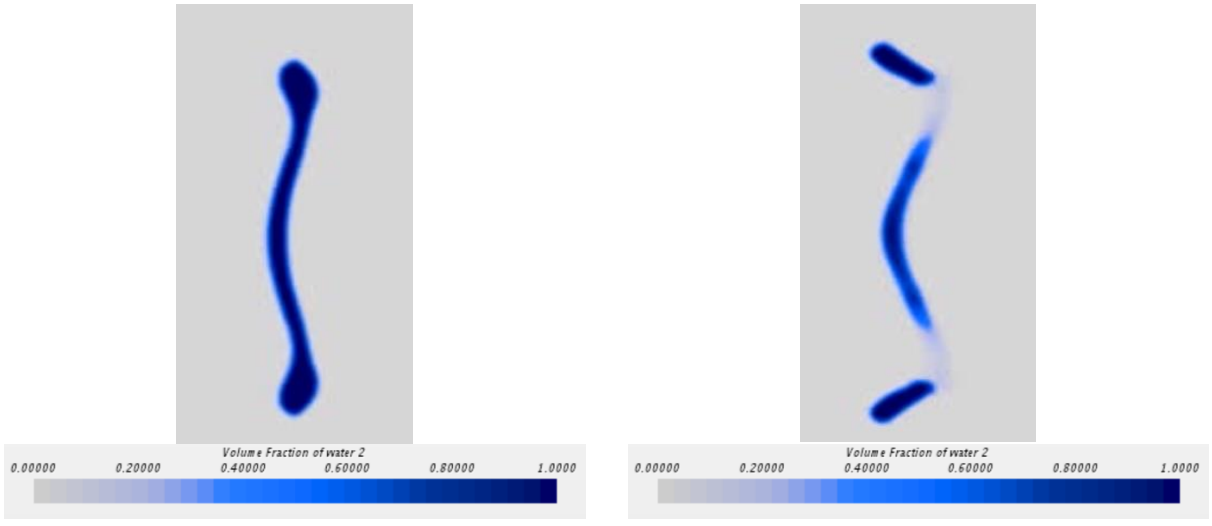

Figure 7: Example of Bag Breakup Regime in Incompressible Gas (We: 17.7139, Solution time: 33.5μs to 40μs)

Figure 7 shows a droplet with the same Weber Number as Figure 6, but in an incompressible gas domain. This droplet seems to undergo a multimode breakup where the main breakup mode is vibrational. It may be undergoing bag breakup as well assuming the model was only successful in developing the rim and not the bag. Something to note here is that the maximum volume fraction of water (seen in the color bars) does not decrease during the solution time like it does in Figure 6.

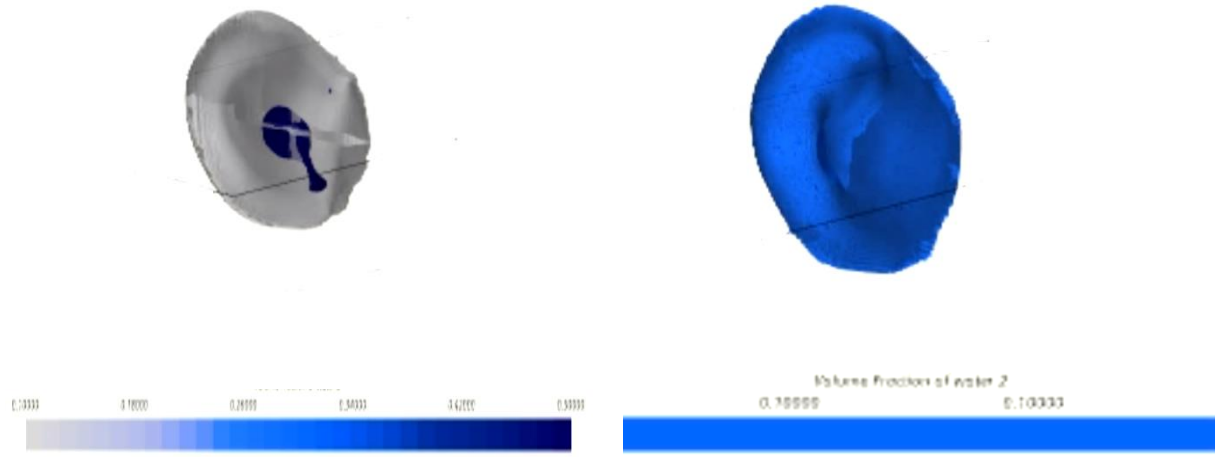

Figure 8: Example of Bag Breakup Regime in 3D Incompressible Gas (We: 17.7139, Solution time: 33.5μs to 40μs)

Figure 8 shows a droplet with the same properties as the droplet in Figure 7, but in a 3D domain. The 3D droplet also does not exhibit a bag, but this may be a result of the isosurfaces being used to view the droplet. The image at 33.5μs provides some evidence of the formation of a bag in the droplet. However, the bag seems to be forming in the opposite of the expected direction. This is due to the air flow switching direction on the opposite side of the droplet.

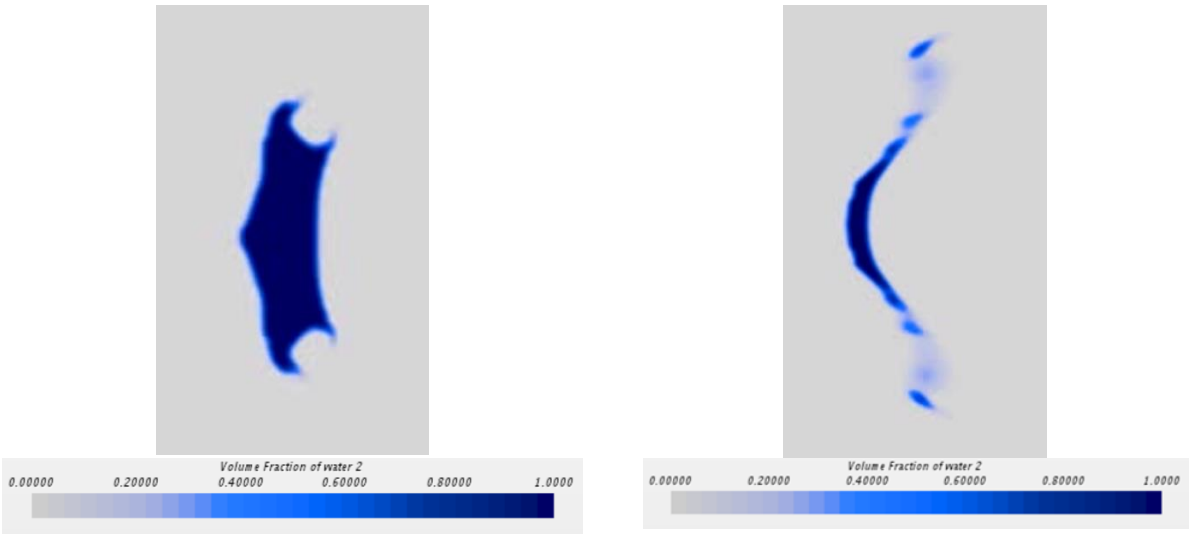

Figure 9: Example of Sheet Stripping in Compressible Gas (We: 130.43860, Solution time: 11μs to 22μs)

Figure 9 above shows an example of sheet stripping. Sheet stripping is qualified here because of the way that layers of water spray off the edges of the droplet, resulting in a droplet that gets smaller over time.

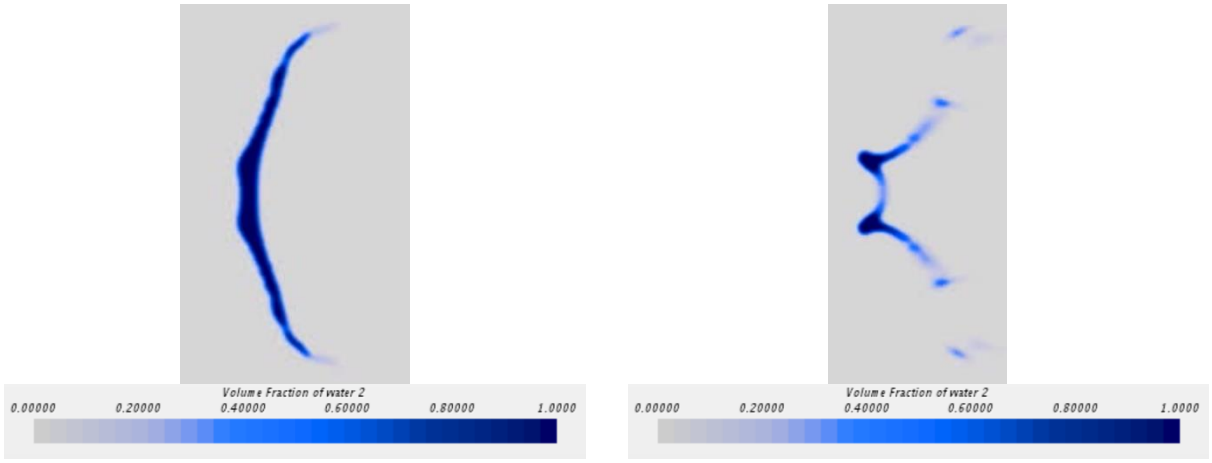

Figure 10: Example of Sheet Stripping in Incompressible Gas (We: 130.43860, Solution time: 28μs to 39μs)

Figure 10 shows a droplet undergoing sheet stripping in an incompressible gas domain. Both Figure 9 and Figure 10 show sheet stripping, but it is clearer in Figure 9. The final solution

in Figure 10 also looks a lot more violent than that of Figure 9. Once again, the maximum volume fraction does not change throughout the solution as it does in Figure 9.

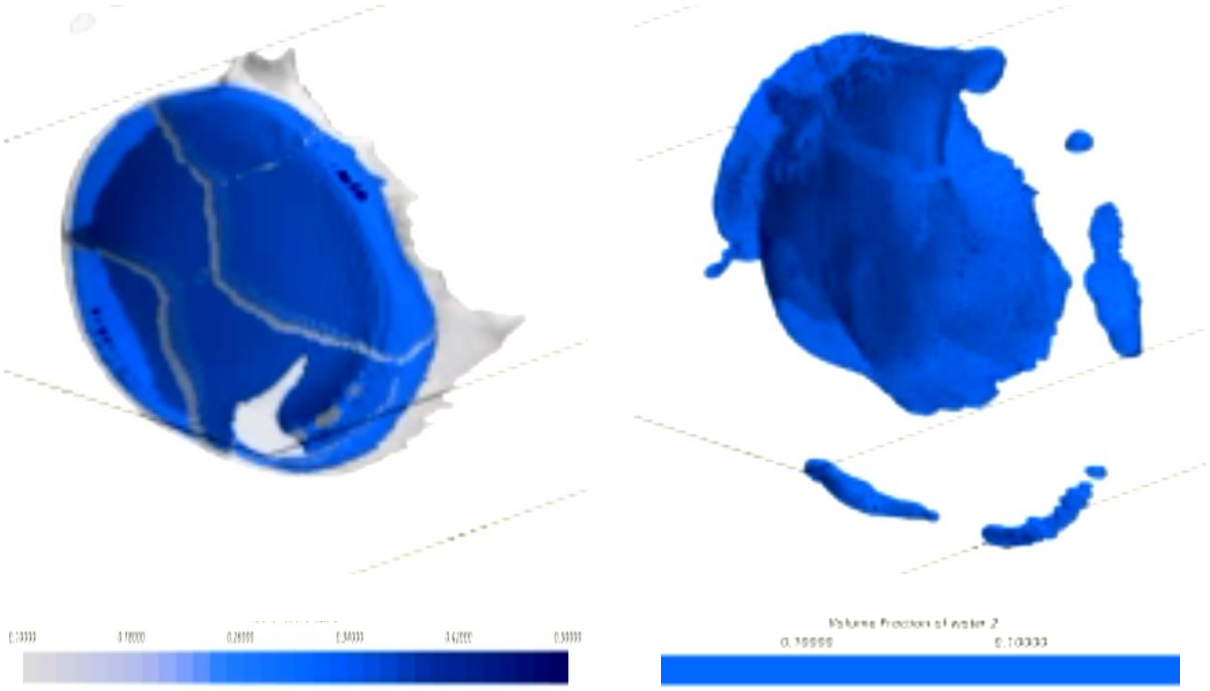

Figure 11: Example of Sheet Stripping in 3D Incompressible Gas (We: 130.43860, Solution time: 28μs to 35μs)

Figure 11 is consistent with Figure 10 in that they both show sheet stripping. However, the isosurface problem is relevant here. Instead of the stripped sheets being tracked as they leave the droplet, they are tracked by the overall volume fraction of the droplet decreasing as more and more water is stripped off the surface of the droplet. The 3D model for sheet stripping does not show properties or geometry that are symmetric about any axis.

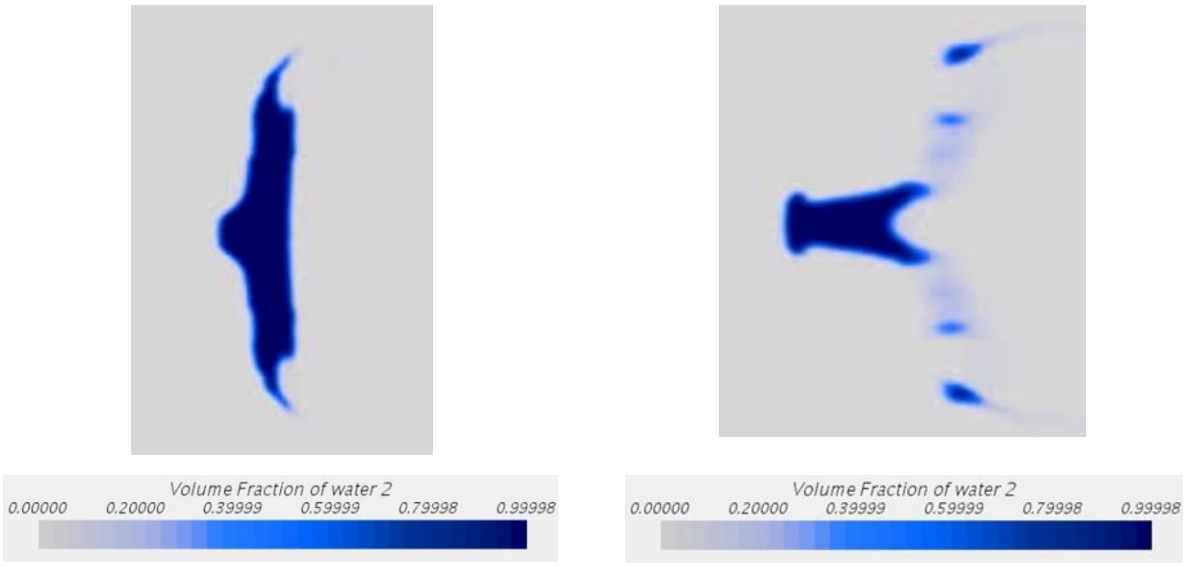

Figure 12: Example of Catastrophic Breakup in Compressible Gas (We: 573.93000, Solution time: 13µs to 26µs)

Figure 12 above shows the progression of a droplet through catastrophic breakup. The catastrophic breakup here is qualified from how the droplet gets spread thin by the air and is sheared apart. The droplet undergoes sheet stripping, and while doing so, also breaks into smaller droplets that experience their own sheet stripping. This sheet stripping happens about 400% faster than it would within the sheet stripping regime

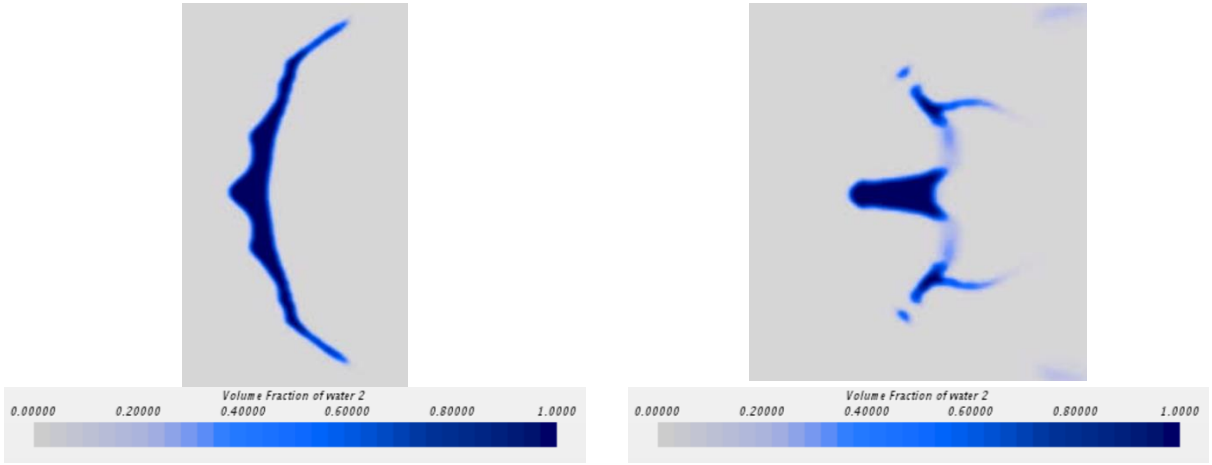

Figure 13: Example of Catastrophic Breakup in Incompressible Gas (We: 573.93, Solution time: 26.5µs to 36.5µs)

Figure 13 more clearly shows catastrophic breakup than Figure 12. In 10 microseconds, much of the water is separated from the droplet. The maximum volume fraction again does not decrease. The second image also shows rotation in the shed water. The main difference between the compressible and incompressible flow here is that the droplet takes longer to break in incompressible flow.

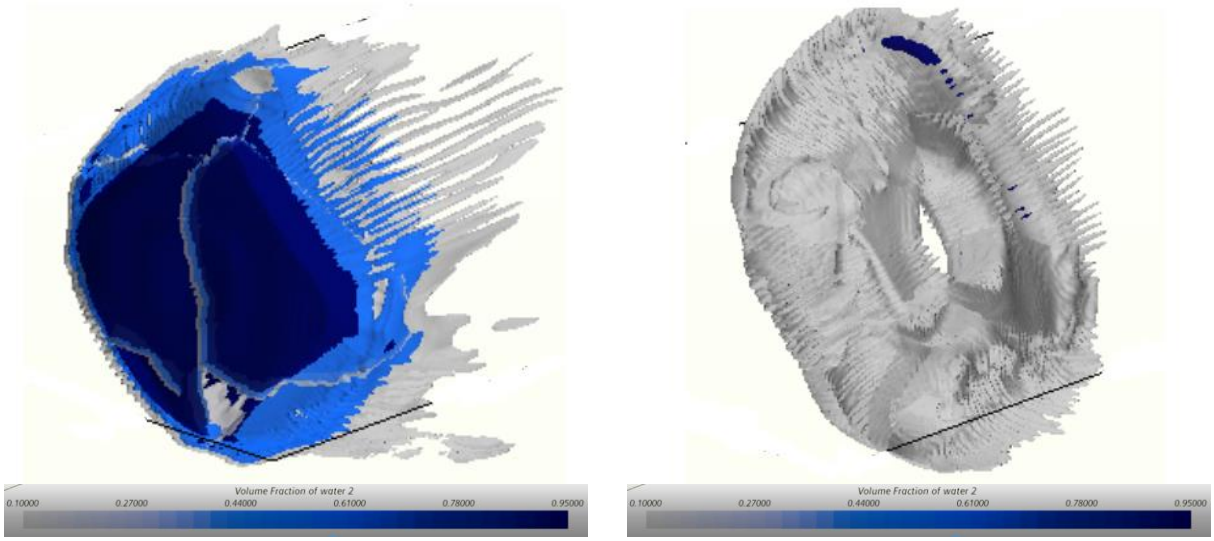

Figure 14: Example of Catastrophic Breakup in 3D Incompressible Gas (We: 573.93, Solution time: 26.5μs to 36.5μs)

The 3D model of catastrophic breakup shows small streams of water coming off the edge of the deformed droplet. This feature was not clear in the axisymmetric cases as the view was limited to a cross section of one edge. However, it looks like a streamer was present on that 2D edge. While the streams are not symmetric in any way, the 2D model was able to show some initial insight on what the streams may look like.

CHAPTER FOUR: DISCUSSION

This section discusses the results from Table 2 starting at lower Weber Numbers and less violent breakup modes and advancing to the higher Weber Numbers and more violent breakup modes.

The compressible studies conducted for Weber Numbers less than 12 all showed characteristics of vibrational breakup; that is, they all showed distinct daughter droplets that formed after the parent droplet split apart. This mechanism is seen clearly in Figure 3. It should be noted that the resolution of the daughter droplets is not perfect, because the residuals for the air phase converge at high values for the solution time in which the daughter droplet forms (around 10 μs to 13.75 μs). The resolution of the daughter droplet is not relevant, as the essential part of this experiment is the breakup mode of the droplet and not any characteristics of the secondary droplets. The incompressible studies mostly agreed with the compressible studies except for We = 5.73 where the droplet in the incompressible regime did not breakup at all and instead stretched and recoiled. Perhaps this indicates a slight shift in the breakup ranges based on compressibility effects of the flow around the droplet.

Many cases near the suggested boundary of vibrational breakup ($We = 12$) showed more than one breakup mechanism. All three test cases within the range $10 < We < 20$ showed characteristics of both vibrational breakup and bag breakup. This finding is contrary to the study conducted by Kadocsa [9] and the study conducted by Chen [11]. However, these findings are supported by Turner's thesis, where it is stated that vibrational breakup can occur in droplets of any Weber Number [10]. The problem with residuals in the case of vibrational breakup was present

in this case as well and may have had a role to play in the combined breakup mechanisms. At Weber Numbers between 20 and 50, the breakup mode was mostly bag breakup. This bag breakup only shows the rim of the bag however, and not the film. This may be because the model is not fine enough, or because of the limitations of the built-in models in Star-ccm+. Another property of the incompressible flows in the bag breakup regime is that the droplet deforms in the opposite direction of what is expected. That is, the rim is convex towards the inlet instead of the outlet. This is likely because of the flow moving behind the droplet and the vectors begin pointing toward the inlet. A major difference between the compressible and incompressible domains here is that the rim for bag breakup in an incompressible gas is a lot more well defined and has more consistent volume fractions in each cell occupied by the droplet. The reason for this likely lies in the numerical methods used by Star-ccm+, especially the root-finding algorithms. These findings suggest that the information in Figure 1 has some validity, at least in this given range.

According to Figure 1, the breakup mode of droplets in the We range of 50-100 is supposed to be bag-and-stamen. However, the simulations conducted for droplets in this range seem to support Chen's claim that this We range should be more generally assigned "multi-mode" breakup [11]. This is true for droplets in the compressible and incompressible domains. The results for this range show mostly a combination of bag breakup and sheet stripping. Not a single droplet in this regime was successful in developing a stamen. Exact reasons for the failure to develop a stamen are not clear. The mesh may have been too coarse, the time-step for the unsteady calculation might have been too large, or the number of inner iterations may have been too little. Residual error dominated the simulations past the initial breakup of the droplet, as they converged at values greater than 0.01 for physical time between 8.75μs and 11.9μs. These large residuals could cause significant errors in the simulation, which could have led to the failure of the droplets to develop

a stamen. The 3D simulations within this range show the center of the droplet decreasing in volume fraction after the rest of the droplet. This lends merit to the idea of bag-and-stamen breakup, but the isosurface issues make this claim difficult to support.

Droplets in the sheet stripping and catastrophic breakup regimes were mostly consistent with Figure 1. While droplets still exhibited properties of their respective breakup mode regardless of air compressibility, the solutions for droplets with the same Weber Number in incompressible and compressible flows still looked vastly different. The incompressible simulation took much longer for the droplet to strip most of itself away, but the compressible simulation droplet maintained its center for much longer. This may be a result of vibrational breakup occurring in the incompressible case, causing the center of the droplet to break apart before the droplet had finished stripping its layers.

The 2D simulations in the catastrophic breakup regime fail to capture some context that highlights the differences between catastrophic breakup and sheet stripping. Without the 3D simulation to show more context, the 2D simulations look like sheet stripping but faster. However, the 3D simulation provides some context in the stream that's seen in the 2D simulation. These streams vary in length and extend around the droplet. This is the clearest example of a 3D droplet showing asymmetric properties about the radial axis of the droplet. These asymmetric droplet properties show how a 2D model would only be accurate for predicting breakup modes, and not for predicting breakup geometry.

The accuracy of the model used in this experiment is reasonable for some breakup modes but questionable for others. For example, vibrational breakup was seen clearly at Weber Numbers less than 12, but for We in the "multi-mode" range, the simulations showed bag breakup along

with other undetermined breakup modes that were lumped into the “multi-mode” classification. Many of these breakup modes are not symmetric and, thus, cannot be captured adequately by an axisymmetric model.

CHAPTER SIX: CONCLUSION

One goal of this research was to develop a computationally inexpensive Lagrangian model of Supercooled Large Droplets for use in ice accretion studies. Another goal of this research was to test this model against experimental models conducted for droplets of similar Weber Numbers in previous literature, such as those seen in Chen [11], Kadocsa [9], and Pilch [13]. One of the biggest difficulties in comparing droplets from laboratory experiments to computational models is that it is difficult to match the exact laboratory conditions in a computational model.

The simulations were carried out successfully for the entire range of Weber Numbers under scrutiny. Errors, such as reverse flow and pressure correction were low or nonexistent for all cases, and residuals were acceptable for the desired time period of droplet breakup; that is, during the phase of primary breakup. These errors unfortunately dominated attempted 3D compressible flows and thus made this data unusable. Some of the breakup modes were not entirely accurate, such as how only the rim was visible for bag breakup, and how a stamen was never fully developed in the regime of bag-and-stamen breakup. The results were at least consistent with the concept of multi-mode breakup [11]. While the simulations did present some problems in the resolutions of the droplets, the breakup modes still fell in the ranges of the previous literature, so the model was accurate to a degree. The results for incompressible flow droplets were different from compressible flow droplets despite having the same Weber Number. Incompressible droplets also had to run about 100% longer to achieve the desired solution. The reasons for the differences between the flows are not entirely clear, however, the density models associated with incompressible flows could have affected the root-finding methods within Star-ccm+, thus causing more differences between the incompressible and compressible flows.

In terms of computational cost, the simulations were very cheap. They were run on two separate systems; a standard desktop computer in parallel with 2 CPU cores, and a server in parallel with 6 CPU cores. The standard desktop could run the 2D simulations in a little under an hour, while the server could run them in as little as 15 minutes. Since incompressible 2D studies took double the amount of time to run to completion, these should certainly be run on more powerful hardware. For the 3D simulations, It would take days to run a simulation on a standard desktop. The 3D model just has too much computational cost associated with it. Despite the AMR reducing the run time, the 3D simulations still took around 8 hours each to run on the server with 6 CPU cores in parallel. The 3D model here is a very general model. Most of the solvers were run on a first-order system and no models besides the ones necessary were selected. More specific situations would call for more specific models and perhaps more accurate results.

The 3D simulations showed that droplets have asymmetric properties at every breakup mode, thus showing that running 2D models is only useful in predicting the actual breakup mode rather than predicting other properties such as breakup geometry, and secondary breakup.

So, for more intense droplet studies, including droplets in shocks, and viscoelastic droplet studies, this model allows a computationally inexpensive starting point. Coupling this model with an Eulerian simulation of a sneeze or cough could offer insight into respiratory droplet breakup, where the initial stage is coupling the Eulerian model with the 2D model presented here to predict initial respiratory droplet breakup. This can be useful in predicting the minimum and maximum distances that primary droplet breakup can cause aerosolized droplets to form.

Star-ccm+'s limitations were clear in these models. The user is limited to specifying the models that are currently supported by Star-ccm+. Future work could use a handmade CFD code

specifically designed to simulate droplets, or something like OpenFoam. Doing this would offer more user control in the numerical methods used for the CFD. This is important to save computational cost as the user could strip away all the flashy parts of Star-ccm+ that cause longer computational time. This would free up computational effort to simulate more accurate droplets in a timely manner. These high-fidelity simulations could also offer insight into secondary droplet breakup, droplets in shocks that affect aircraft, and respiratory droplets.

REFERENCES

[1] "In-Flight Icing Encounter and Loss of Control Simmons Airlines d.b.a. American Eagle Flight 4184" Vol. 1, National Transportation Safety Board, 1994.

[2] O'Rourke, P. J., and Amsden, A. A. "The Tab Method for Numerical Calculation of Spray Droplet Breakup" *1987 SAE International Fall Fuels and Lubricants Meeting and Exhibition*. SAE International, 1987.

[3] Jeck, R. K. "Icing Design Envelopes (14 CFR Parts 25 and 29, Appendix C Converted to a Distance-Based Format" *14 C.F.R.*, Office of Aviation Research Washington, D.C. 20591, 2002.

[4] Cober, S., Isaac, G., Shah, A., and Jeck, R. "Defining Characteristic Cloud Drop Spectra From In-situ Measurements" *41st Aerospace Sciences Meeting and Exhibit*.

[5] Politovich, M. K. "Aircraft Icing Cuased by Large Supercooled Droplets" *Journal of Applied Meteorology* Vol. 28, No. 9, 1989, pp. 856-868.doi: 1520-0450(1989)028<0856:AICBLS>2.0.CO;2

[6] Wright, W. "LEWICE User's Manual" Vol. Version 3.2, NASA, Cleveland, OH, 2008.

[7] Siemens. "STAR-CCM+ User's Manual." 13.06.012 ed., Simcenter.

[8] Hsiang, L.-P., and Faeth, G. "Drop deformation and breakup due to shock wave and steady disturbances" *32nd Aerospace Sciences Meeting and Exhibit*.

[9] Kadocsa, A., Tatsch, R., and Krist'of, G. "Analysis of Spray Evolution in Internal Combustion Engines Using Numerical Simulation" *Journal of Computational and Applied Mechanics* Vol. 8, No. 1, 2007, pp. 85-100.

[10] Turner, J. "An evaluation of computational methods to model large droplet secondary breakup," *DEPARTMENT OF AEROSPACE ENGINEERING AND ENGINEERING SCIENCE AND MECHANICS*. Vol. Aerospace Engineering and Engineering Science, Pennsylvania State University, Schreyer Honors College, 2017, p. 1 electronic document.

[11] Chen, Y., DeMauro, E. P., Wagner, J. L., Arienti, M., Guildenbecher, D. R., Farias, P., Grasser, T. W., Sanderson, P., Albert, S., Turpin, A., Sealy, W., and Ketchum, R. S. "Aerodynamic Breakup and Secondary Drop Formation for a Liquid Metal Column in a Shock-Induced Cross-Flow," *55th AIAA Aerospace Sciences Meeting*.

[12] Profir, M. "Automated moving mesh techniques and re-meshing strategies in CFD applications using morphing and rigid motions" CRS4, 2012.

[13] Pilch, M., Erdman, C. A., Reynolds, A. B., U.S. Nuclear Regulatory Commission. Office of Nuclear Regulatory Research. Division of Accident Evaluation., and University of Virginia. Department of Nuclear Engineering. *Acceleration induced fragmentation of liquid drops*. Washington, D.C.Springfield, Va.: The Commission : Available from GPO Sales Program, Division of Technical Information and Document ControlNational Technical Information Service, 1981.